RADIANT HEATER DESIGN TO SIMULATE RE-ENTRY AERODYNAMIC HEATING

M.Y. Abdollahzadeh Jamalabadi[1,2,3*] & M. Dousti[4]

[1] Assistant Professor Maritime University of Chabahar, Chabahar, mail.Box:99717-56499, Iran

[2] Shanghai Key Lab of Vehicle Aerodynamics and Vehicle Thermal Management Systems, Tongji University, Shanghai, China

[3] K.N. Toosi University of Technology, Tehran, Iran

[4] Faculty of Engineering, Zanjan University, Zanjan, Iran

ABSTRACT

Experimental simulation of heat transfer through the re-entry of space vehicles are in the interest field of areo-engineers. The purpose of the current study is to experimentally and numerically investigate the effect of thermal radiative heat sources (Quartz lamps) on thermal heating of a thin plate inside an open cavity. The enclosure is open on the sides and is cooled from the bottom wall. The top wall of the enclosure is acting as a thin plate. The heating elements are placed at a distance from the bottom wall inside the cavity. The effects of various factors, such as plate distance from the heat source, the heat source strength, and the thermal radiative emissivity on plate temperature distribution is measured and a correlation for the plate maximum temperature for a single lamp is presented. Using that correlation a method is presented to estimate the maximum temperature of a heated thin plate in an open cavity exposing an arbitrary heating lamps power and arrangement. Good agreements between the experimental and the estimated results are gained. To reduce the number of experiments a finite-volume code which solves the governing nonlinear differential equations (mass, momentum, energy of fluid, and energy of surface) based on Patankar's SIMPLE method is developed and is benchmarked by experiments. By the code the length of uniform temperature region as a function of heat source number, plate distance from the heat sources, distance between heat sources, and the uniformity coefficient is calculated.

Keywords: *Open cavity, Surface radiation, Natural convection, Experimental correlation, uniform thermal loading, Infrared camera.*

1. INTRODUCTION

When a hypersonic vehicle, such as a planetary-entry capsule or a high-lift reentry vehicle Space Shuttle or a scramjet-powered aircraft, is designed to fly outside the region of the earth's atmosphere for distances of 5000 miles or near the outer edge of the atmosphere; it reenter the atmosphere with a large amount of kinetic energy due to its high velocity at suborbital speediness of from 20,000 to 22,000 ft/s and a large amount of potential energy due to its high altitude. At such high velocities, the aerodynamic heating of the reentry vehicle becomes severe because it needed that at the earth's surface it contains no kinetic or potential energy ($Q_{total} \approx 0.5\ C_f / C_D\ KE$). Since the shuttle must slow down early during reentry into the earth's atmosphere to avoid massive aerodynamic heating. Therefore, with the purpose of obtain this deceleration; a high drag is desirable for the space shuttle. In addition, the pointed-nose reentry body is doomed to failure because it would burn up in the atmosphere before reaching the earth's surface. To minimize aerodynamic heating ($C_f << C_D$), one actually wants a blunt (Drag mainly should be due to pressure drag rather than friction drag) rather than a slender body (the maximum *L/D* ratio, 6+ $12/M_\infty$, of the space shuttle during reentry is about 2) [1].

Other than shuttles, the hypersonic vehicles for sustained hypersonic flight in the atmosphere are a major challenge to the next generation of aerospace engineers (the X-43 Hyper-X test vehicle powered by a supersonic combustion ramjet engine, achieved sustained flight for 11 s at Mach 6.9 in 2004). The aerodynamic heating rate varies as the cube of the velocity ($Q_w / A \approx 0.5\ \rho_\infty\ C_H\ V^3 \approx 0.25\ \rho_\infty\ C_f\ V^3$) is in contrast to aerodynamic drag, which varies only as the square of the velocity. Even ambient density at a height of about 74 km is not much more than one millionth of sea-level density, the Shuttle Orbiter experienced peak heating. Since the nose region of high-speed blunt bodies is of practical interest in the calculation of drag and aerodynamic heating ($q_w \approx R^{-1/2}$), the properties of the flow behind the normal portion of the shock wave take on some importance. Because when a shock wave impinges on the boundary layer, flow separation and local reattachment may occur, creating local regions of high heat transfer. As the stagnation point heating varies inversely with the square root of the nose radius; hence to reduce the heating, increase the nose radius ($q''_w \approx 1.83 \times 10^{-12}\ \rho_\infty^{1/2}\ V^3 R^{-1/2}(1 - 2c_pT_w / V^2)$). The static temperature ratio across a normal shock wave with M_∞ = 36 is 42. It means if the air be at 258 K the surface would be at 11000 K. Since thermal

radiation from the hot gas becomes a substantial portion of the total heat transfer to the body surface. In the design of the Apollo heat shield, the portion of radiation to the total heat transfer to the body surface was considered 0.3.
In the history of flight, the most unfortunate example of such destruction occurred on February 1, 2003, when the space shuttle Columbia crumbled over Texas during entry into the earth's atmosphere. Several of the thermal shield tiles near the leading edge of the left wing had been damaged by debris during launch. This allowed hot gases to penetrate the surface and destroy the internal wing structure [3].
The design of thermal system at high temperature occurs in applications such as thermal control of electronic systems [1], transformers [2], fusion reactors technology [3], hot structures [4] , fuel cells [5], fibrous insulations [6], solar-energy drying systems[7], chemical vapor deposition reactors[8], smoke diffusion in a fire outbreak in building [9], flame [10],automotive [11], and HVAC [12]. Several investigations have been carried out on natural convection in open cavities [13-14] but few papers have investigated the combined heat transfer by natural convection and thermal radiation in open cavities, as stated in Ref.[15]. Representative studies may be categorized depending on the aim of experiment to obtain the fluid dynamic behavior using visualization techniques [16-17], temperature distribution of fluid [18-20] ,both fluid flow and flow temperature [21-23] , maximum temperature of solid surface[24-27], heat flux through the fluid [28], heat flux on the solid surface[29-31].
Also considerable attention has been given to numerical investigation of natural convection from enclosures with discrete heat sources attached on the walls and their optimal distribution [32-35]. Recently the effect of thermal radiation in an enclosure with discrete heaters buoyant in the fluid (not attached to the solid wall like electronic boards) is investigated numerically [36-51].To date no data is available on the experimental investigation of the effect of the thermal radiation in an enclosure with discrete heaters as heating object to model a thermal loading system. Also there is no numerical investigation to uniform heating of a plate by discrete heat source.

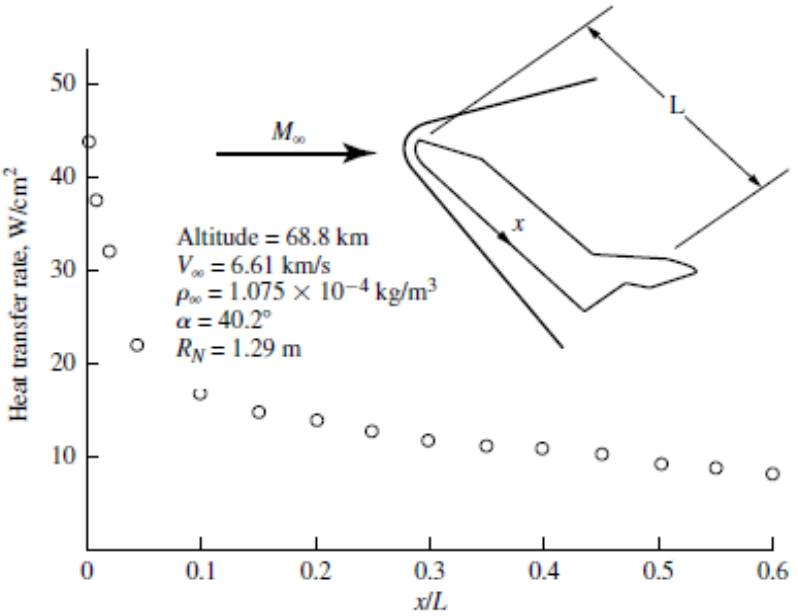

Figure 1. Required heating of a sample shuttle as a function of its distance from nose.

2. EXPERIMENTAL RIG

Figure 1 show the required heating of a sample shuttle as a function of its distance from nose which the conditions are mentioned in the figure. To do that an experimental setup in Cartesian coordinate system is considered.
Figure 2 shows the schematic of the experimental set-up. As shown, a thin plate is mounted horizontally on the four supports in its corners above the quartz lamps. The carbon-steel plate thickness is 3 mm and its surface dimension is 100×100 cm. The Quartz lamps (BLV Licht - und Vakuumtechnik GmbH, halogen flood light lamps, 2000 W, 230 V, 44000 lm, 3000 K) are acting as heaters. The power of the each Quartz lamp is changed by an industrial dimmer (TD30 Tesla company, 1500VA, 15A) through the experiment. The distance of the heater from the plate is varied by variation in the supports heights. In addition, the plate emissivity changes by painting the plate. The range of the heater powers, distances from the plate and their emissivity are given in Table 1. In order to control the temperature of the quartz lamp's electric connections through the experiment, cold water maintains circulated through the bottom wall of the enclosure. Thermal insulator (Luyang bricks and ceramic fiber textile) is used to insulate and constrained the two sides of the cavity which is perpendicular to the Lamps direction. Air ventilates through the two sides of the

cavity which is parallel to the Lamps direction (openings in Figure 2). The set up uses a ThermoProTMTP8 infrared camera (8μm-14μm bandwidth, temperature range -20°C to 800°C) to measure the surface temperature evolution while the plate is heated by Quartz lamp. The camera is placed normal to the thin plate surface in the distance of 1 meter above it (see Figure 2). The infrared camera is connected to a 12 bit data acquisition with real time software. The camera captures 10 frames per seconds.

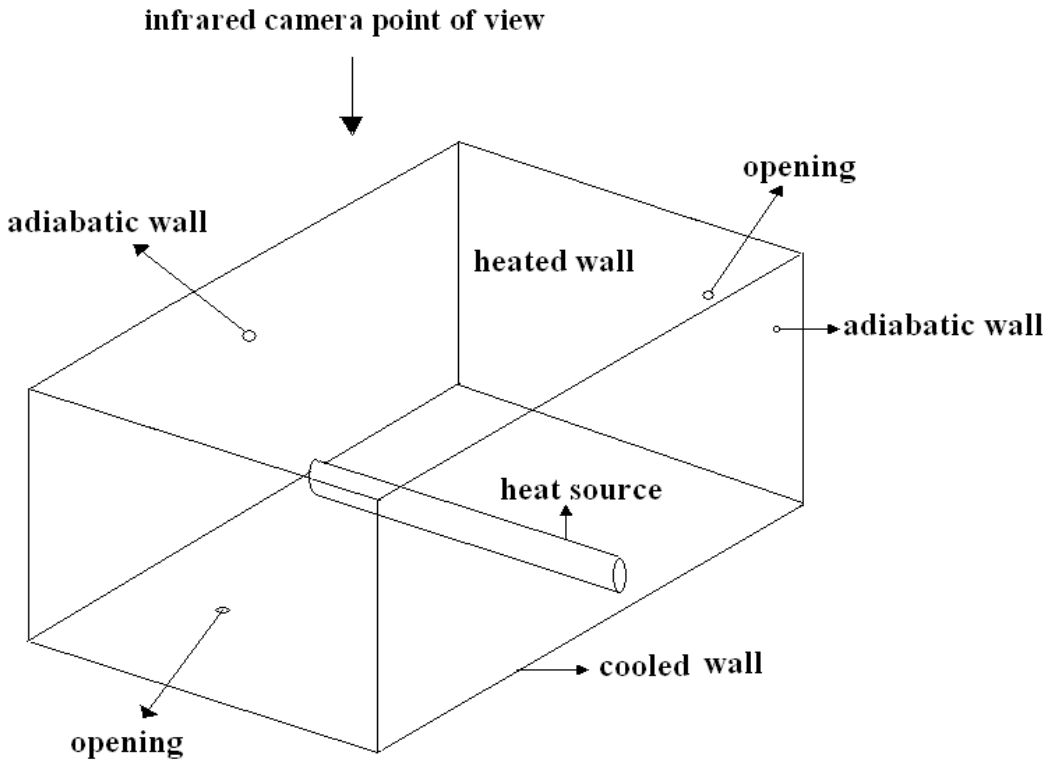

Figure 2. Schematic of the experiment: enclosure with discrete heaters and boundary conditions.

Table 1. Range of parameters considered in this study

parameter	Range in Experiment	Range in Numerical Calculation
Q	200-2000 (watt)	100-2000 (watt)
H	3.5-19.5 (cm)	3.5-19.5 (cm)
D	1 (cm)	1 -20(cm)
ε	0.576-0.889	0-1
N	1-3	1-20
T_∞	300 (K)	300 (K)

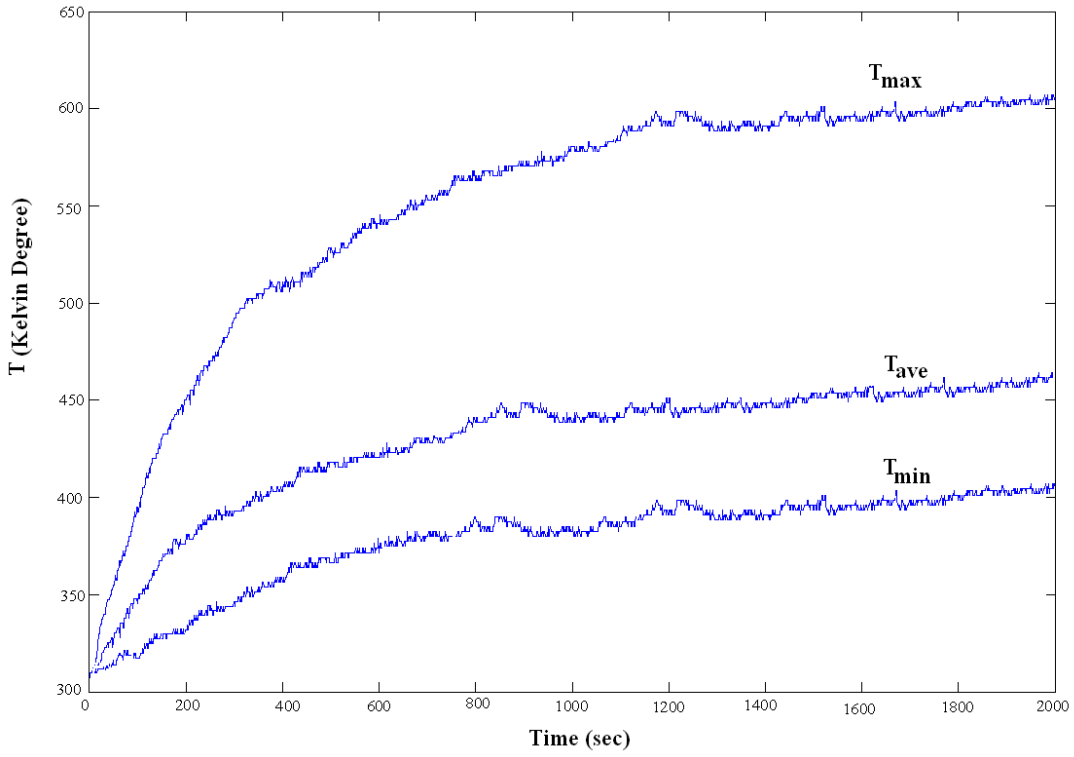

Figure 3. Maximum, average and minimum temperature variation of the heated plate versus time to achieve steady state condition (h=3.5 cm, Q = 2000 watt)

3. ONE LAMP HEATING

3.1 PRE-TEST

At the pre-test step of the experiment some thermocouples (type K) used to verify the precision of infrared camera and to measure the temperature difference between two sides of thin plate. As measured by the thermocouple devises the maximum temperature difference between top (unexposed to the heat flux) and bottom (exposed to the heat flux) of thin plate which occurs at the maximum heat flux position of the plate (equals the maximum temperature point corresponds to the midpoint of the heater) is less than 5 degree of Celsius. For the engineering application we the difference between the top and bottom of the plate temperature can be neglected and the top plate temperature which measured by infrared camera is considered as the temperature of thin plate. The error calculation is shown Table 2. As shown the maximum relative measuring error is 0.6 %.

3.2 DATA ACQUISITION

Figure 2 depicts the maximum, the average and the minimum temperature of the heated plate when plates are placed at 3.5 cm of a 2000W heater (h=3.5 cm and Q = 2000). As shown by the Figure 3 Temperature reaches to a steady value after 1000 seconds. However for more accuracy the experiment time is extended to 2000 seconds. For thermal design purposes the experiment focuses only on the maximum temperature of the heated plate. A code is developed for data transformation of Infrared images to plot the temperature contours (Surface temperature image of the thin plate that is taken by the Infra-red camera). The spatial resolution of the image which captured by the IR camera is 384x288 RGB points. In Figure 4 the contour of temperature on the heated plate is shown. The temperature values are in degree of Celsius and the unit of coordinate systems in millimeters. The isotherm lines are parallel with the heat source orientation as illustrated in the Figure 4. This demonstrated the effectiveness of adiabatic walls that are provided perpendicular to heat source to observe the effect of natural convection ventilation in a one direction.

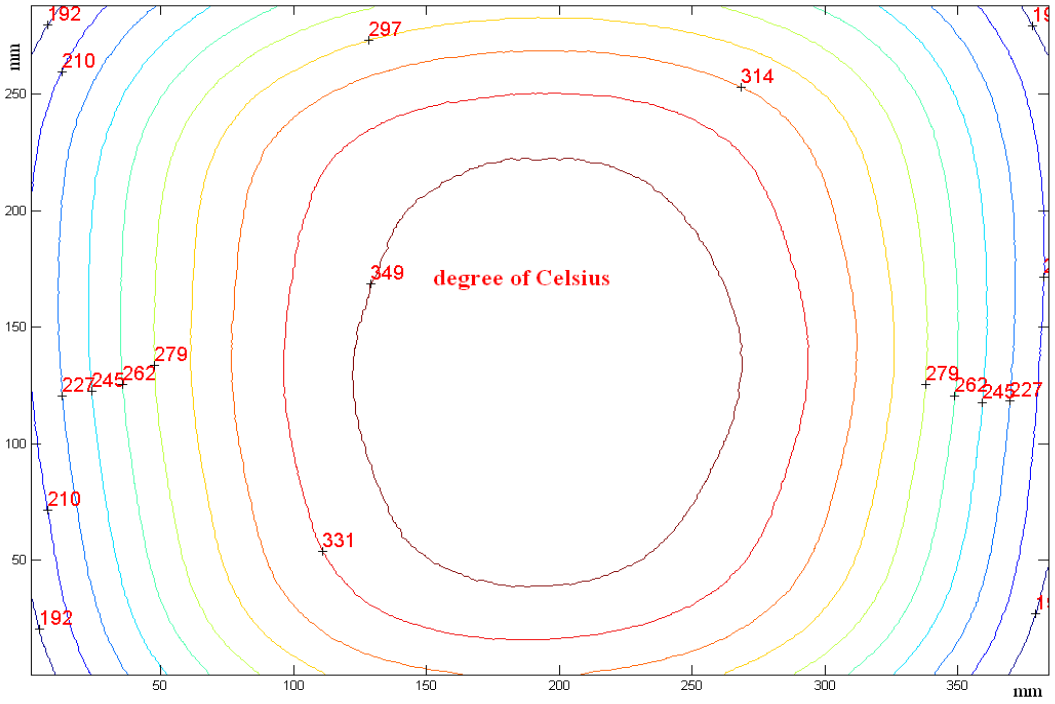

Figure 4. Contour of temperature on the heated plate

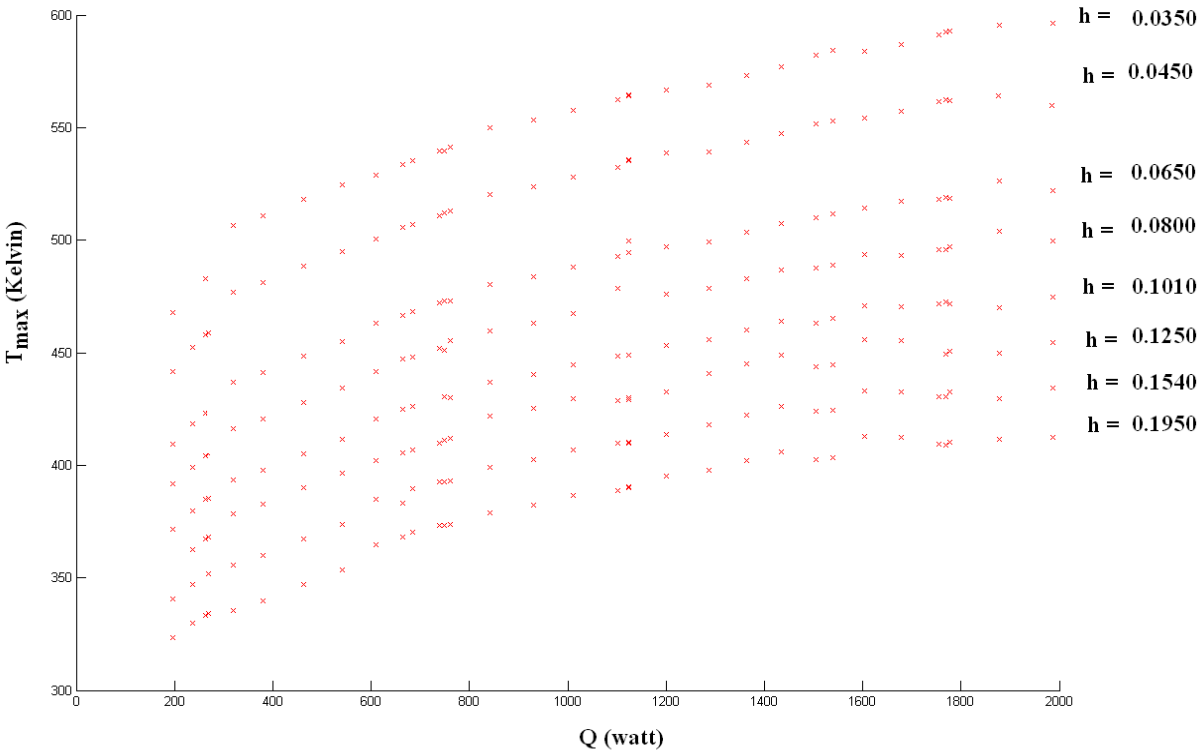

Figure 5. Maximum Temperature of the heated plate as a function of heat source power for various height of the plate

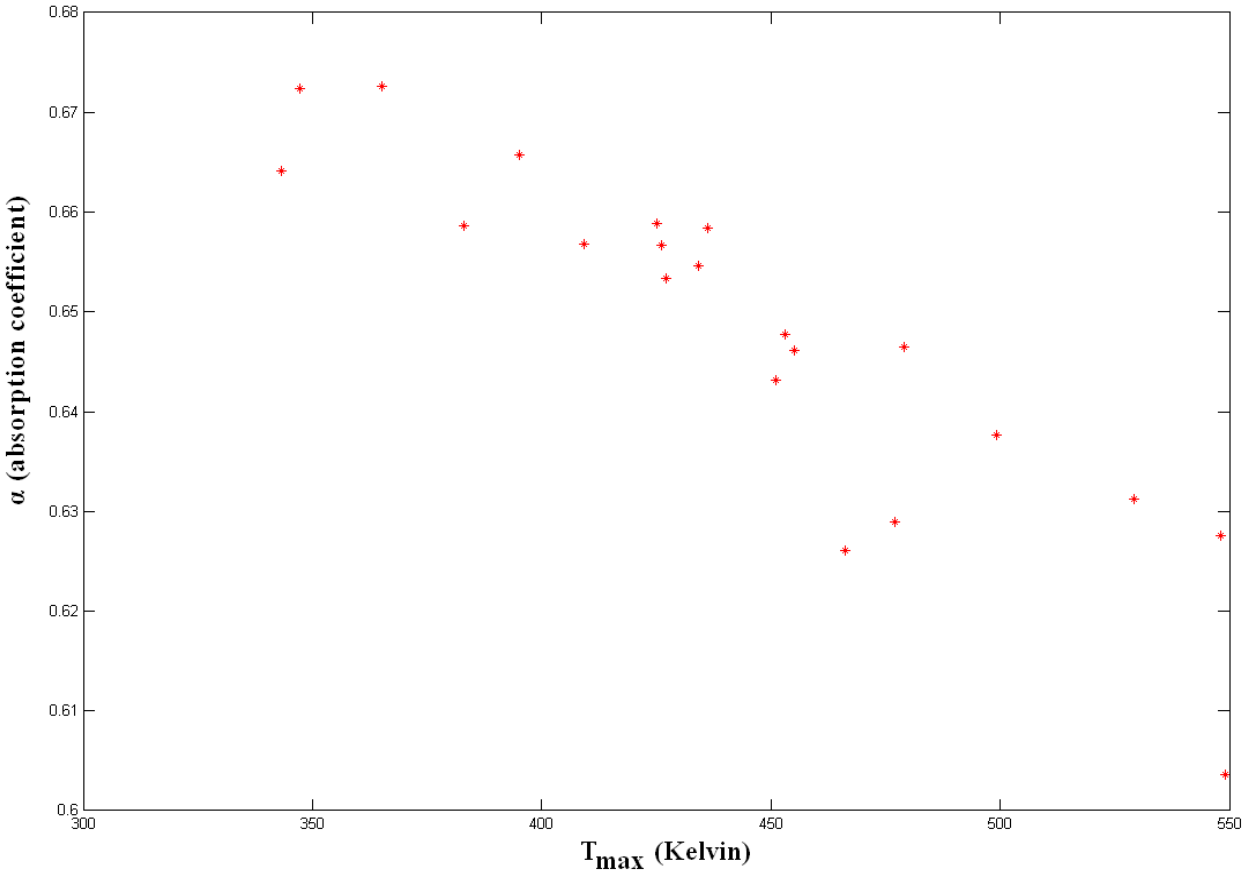

Figure 6. Relative absorbtion coefficient of unpainted steel and black painted as a function of Temperature

3.3 Experimental Correlation

The Figure 5 shows the maximum temperature of the heated plate as a function of heat source power for various height of the plate. The plate has painted by the black color (Dupli-color exhaust paint Supertherm which is temperature-resistant up to 800°C). As shown through the 168 experiments (21 levels of power and 8 levels of height) by increase of heat source power the maximum temperature increase. However decrease in distance between heat source and the heated plate leads to increase in temperature. By a regression analysis on the data we reach the following empirical correlation:

$$T_{\max} = 120.2\mathrm{Q}^{0.119} H^{-0.212} \quad (1)$$

with root square error of 99.3%. Since measured variables in Equation (1) have uncertainty, the first step is assessing the experimental uncertainties of measured temperature. The total error of temperature is a sum of the error in any component, error of the measured value, i.e.,

$$\frac{\Delta T_{\max}}{T_{\max}} = 0.119\frac{\Delta \mathrm{Q}}{Q} + 0.212\frac{\Delta H}{H} \quad (2)$$

based on the computation of the error estimation of parameters of single quartz lamp measurements which is shown in Table 2 and the above formula the relative error of temperature measurement is 0.0063. So the precision of empirical correlation of Eq. (1) in temperature estimation is 98.7 %. By more tolerance the more justified correlation is obtained as:

$$T_{\max} = 128.9\left(\frac{\mathrm{Q}}{H^2}\right)^{0.1075} \quad (3)$$

in this semi-empirical correlation coefficients obtained with 95% root square error. The same error analysis calculated for Equation (3) is performed for this equation the precision of empirical correlation of Eq. (3) in temperature estimation is 94.3 %.

Table 2. Computation of the error estimation of parameters of single quartz lamp measurements

parameter	Minimum value	Maximum error	Maximum Relative error
Q	200 (watt)	1 (watt)	0.005
H	3.5 (cm)	0.1 (cm)	0.0286
D	1 (cm)	0.01 (cm)	0.01
ε	0.576	0.001	0.0017
N	1-3	0	0

3.4 EMISSION COEFFICIENT MEASUREMENT

The devise used for determining emittance of painted and unpainted plate is a portable infrared reflectometer the AzTek [AZ Technology] Temp 2000 as suggested in Reference [38]. AZ Technology's TEMP 2000A handheld emissometer/reflectometer is the recognized replacement for an aging Gier-Dunkle DB100. Measurement accuracy of this devise (for secular and diffuse samples) is ± 1% of full scale for gray samples and repeatability is ± 0.5% of full scale or better. The emissivity of the painted plate with black paint is 0.889, the emissivity of the unpainted plate is 0.576 ,and the emissivity of reflector is 0.04. At the next stage of experiment the same plate is used but with the natural color of clean carbon steel. The absorbtion coefficient in thermal radiation physics defined as the fraction of a thermal irradiation absorbed by the surface of the absorber:

$$\alpha = \frac{q''_{abs}}{q''_{irradiate}} \qquad (4)$$

If we neglect the effect of convection and conduction against radiation ,the heat transfer gained by plate to receive the temperature is controlled by plate absorbtion coefficient. So From Eq (3) ($T_{\max} \propto q''$) and (4) the relative absorbtion coefficient of carbon steel plate to black plate can found by the relation

$$\frac{\alpha_{cs}}{\alpha_{black}} = \left(\frac{T_{\max}}{128.9}\right)^{7.2765} \frac{H^2}{Q} \qquad (5)$$

Some experiment is performed to get the relative absorbtion coefficient of clean(unpainted) and black carbon steel plate by Eq(5). In Figure 6 absorbtion coefficient of steel as a function of temperature is presented. As demonstrated absorbtion coefficient of carbon steel plate has the value between 0.6 and 0.7. It could be approximated by the value of 0.65 with the 0.05 uncertainty. As illustrated in Figure 6 the emissivity of unpainted plate decreasing slightly by increase of temperature. As shown in Figure 6 the relative emissivity of unpainted plate to painted plate is 0.66 and by precise calculation at room temperature the relative emittance is 0.65. This experiment shows the validity and applicability of the proposed correlation (Eq(5)) and a method to calculating absorbtion coefficient of thin plates at high temperature which cannot be detected by ordinary devises (such as portable infrared reflectometer the AzTek [AZ Technology] Temp 2000).

4. ARBITRARY THERMAL LOADING

In previous section the effect of one heat sources on a plate temperature have been studied because the effect of complex arrangement of heat sources on plate temperature is a nonlinear combination of an each lamp results. In this section a rule of thumbs for engineering application is developed (which is not requested complicated CFD calculations) to calculate the maximum temperature of thin plates heated by quartz lamp discrete heat sources. For an arbitrary arrangement of heat sources first the C_{ij}, view factor corrections of a source i at the position of maximum temperature j, should be defined for each of heat source. Then effective power for using in Equation (1) calculated as bellow

$$Q_{eff} = \sum_{heat\ sources} Q_i C_{ij} \quad (6)$$

when the normal distance of heat sources from the plates are equal. But at the other cases the effective heat flux for using in Equation (3)can be calculated as follow

$$\left.\frac{Q}{H^2}\right|_{eff} = \sum_{heat\ sources} \left.\frac{Q}{H^2}\right|_i C_{ij} \quad (7)$$

Table 3. Case Studies for various arrangement of Quarts Lamps

H(m)	P_1(watt)	P_2(watt)	P_3(watt)	Maximum Temperature (K)	Relative error of Eq(1)	Relative error of Eq(3)	Relative error of Eq(19)
0.045	397	0	0	470.15	0.0056	0.0161	0.0067
0.045	397	782	0	545.15	0.0204	0.0218	0.0214
0.045	397	782	629	560.15	0.0061	0.0114	0.0077
0.045	1900	782	629	600.15	0.0037	0.0159	0.0064
0.045	0	782	629	557.15	0.0219	0.0252	0.0231
0.045	0	1866	629	577.15	0.0131	0.0028	0.0107
0.045	0	1866	0	549.15	0.0351	0.0274	0.0331
0.035	0	298	0	481.15	0.0016	0.0162	0.0088
0.035	417	298	0	525.15	0.0045	0.0103	0.0102
0.035	417	298	366	569.15	0.0455	0.0428	0.0405
0.035	0	237.6	0	466.15	0.0064	0.0237	0.0140
0.035	0	244	0	475.15	0.0096	0.0071	0.0021
0.035	269	244	0	520.15	0.0257	0.0163	0.0195
0.035	269	244	257	536.15	0.0249	0.0185	0.0192
0.035	269	0	257	504.15	0.0226	0.0105	0.0160
0.035	269	0	0	477.15	0.0022	0.0135	0.0051
0.035	738	0	0	546.15	0.0170	0.0131	0.0117
0.035	738	0	782	568.15	0.0157	0.0156	0.0110
0.035	738	715.2	782	609.15	0.0256	0.0311	0.0219
0.035	0	715.2	0	546.15	0.0207	0.0164	0.0153
0.044	102	71	42	463.15	0.0640	0.0458	0.0612
0.044	429	245.2	440	540.15	0.0308	0.0298	0.0309
0.044	688	245	762	565.15	0.0288	0.0322	0.0296
0.044	688	1058.4	762	603.15	0.0371	0.0457	0.0388
0.044	0	1058	0	550.15	0.0297	0.0305	0.0300
0.079	716	0	734	491.15	0.0154	0.0204	0.0289
0.058	716	0	734	521.15	0.0180	0.0212	0.0246
0.043	716	0	734	548.15	0.0192	0.0201	0.0190
0.042	716	0	734	550.15	0.0191	0.0199	0.0185
0.212	704	0	720	397.15	0.0044	0.0131	0.0394
0.173	704	0	720	416.15	0.0084	0.0163	0.0388
0.136	704	0	720	438.15	0.0111	0.0181	0.0364
0.107	704	0	720	462.15	0.0160	0.0221	0.0360
0.079	704	0	720	492.15	0.0195	0.0243	0.0329
0.045	742	716	0	567.15	0.0355	0.0391	0.0368
0.047	742	716	0	562.15	0.0352	0.0390	0.0374
0.060	742	716	0	533.15	0.0311	0.0359	0.0386
0.079	742	716	0	503.15	0.0295	0.0352	0.0429
0.107	742	716	0	471.15	0.0268	0.0336	0.0467
0.136	742	716	0	445.15	0.0204	0.0280	0.0455
0.172	742	716	0	422.15	0.0168	0.0251	0.0470
0.212	742	716	0	401.15	0.0099	0.0190	0.0448

In Table 3 the distance of three lamps from the thin plate , the power of each lamp, the maximum temperature measured by experimental , and the error of calculated maximum temperature by each proposed methods (based on the empirical and semi-empirical relations) for 42 cases are shown. The distances between lamps are 2.5 centimeters. However the fitted curve in equation (1) has less error in computing maximum temperature than Equation (3) in one lamp heating and in complex thermal loading but the method which used the Equation (3) can be generalized for thermal heating with various heights and is more justified.

5. NUMERICAL SIMULATION

5.1 MATHEMATICAL MODEL AND BOUNDARY CONDITION

The schematic of the open cavity is shown in Figure 7.This 2D cavity is a cross section from the middle of 3D cavity shown in Figure 1.As shown the lower wall is at constant temperature while the upper wall is adiabatic. The heaters are installed at a distance from the bottom wall of the cavity. The energy generated by the discrete heaters is removed from the cavity by air circulation. In writing the governing mass, momentum and energy equations the following assumptions are made: the flow is laminar, fluid is Newtonian, viscous heat dissipation is neglected, walls are diffuse and gray(Absorbtion coefficient is equal to emission ie $\alpha=\varepsilon$), and the fluid is a non-absorbing medium. All thermo-physical properties are constant except density, which varies linearly by Boussinesq approximation. Followings are the non-dimensional governing mass, momentum and energy equations, respectively:

$$\frac{\partial U}{\partial X}+\frac{\partial V}{\partial Y}=0 \tag{8}$$

$$U\frac{\partial U}{\partial X}+V\frac{\partial U}{\partial Y}=\frac{-\partial P}{\partial X}+\Pr\nabla^2 U \tag{9}$$

$$U\frac{\partial V}{\partial X}+V\frac{\partial V}{\partial Y}=\frac{-\partial P}{\partial Y}+\Pr\nabla^2 V+Ra\Pr\theta \tag{10}$$

$$U\frac{\partial \theta}{\partial X}+V\frac{\partial \theta}{\partial Y}=\nabla^2\theta \tag{11}$$

$$\sum_{j=1}^{n}(\delta_{ij}-F_{ij})\Theta_j^4=\sum_{j=1}^{n}(\delta_{ij}-(1-\varepsilon_j)F_{ij})\frac{\zeta_j}{\varepsilon_j} \tag{12}$$

As shown in Figure 7, the boundary conditions for the system are:
On bottom wall surface (Y=0):

$$U=V=0\ \frac{\partial P}{\partial Y}=0\ \ \Theta=1\ \ \varepsilon=0.04 \tag{13}$$

On top wall (Y=A):

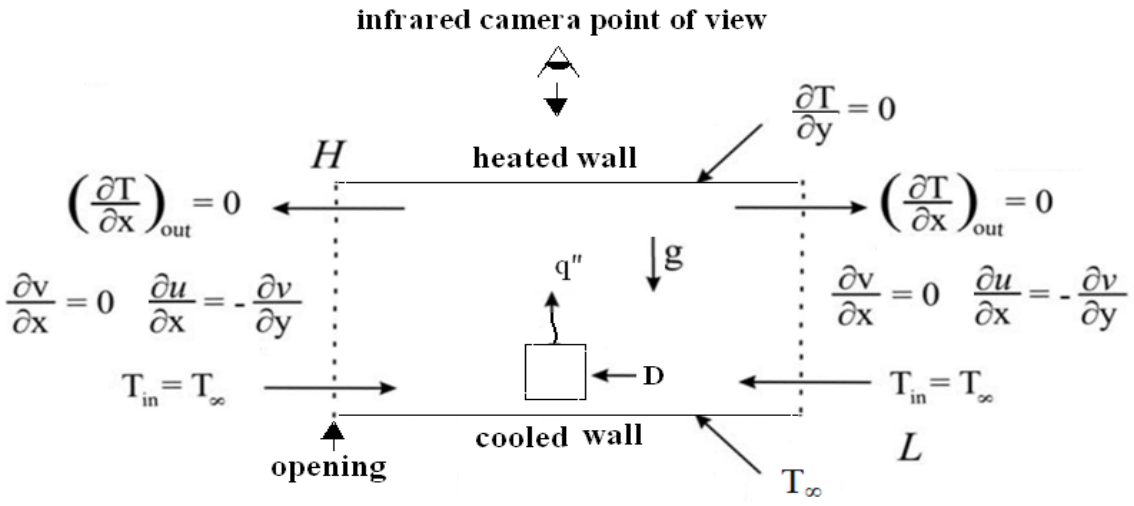

Figure 7. Schematic of the enclosure with discrete heaters, the coordinate system and boundary conditions

$$U=V=0 \quad \frac{\partial P}{\partial Y}=0 \quad \frac{\partial \Theta}{\partial Y}=0 \quad \varepsilon_{cs}=0.576 \quad \varepsilon_{black}=0.889 \tag{14}$$

On the heaters:

$$U=V=0 \quad \frac{\partial P}{\partial Z}=0 \quad \frac{\partial \Theta}{\partial Z}=-Bi^{*}\zeta_{0} \quad \varepsilon=1 \tag{15}$$

On the symmetry line (X=0):

$$\frac{\partial P}{\partial X}=0 \quad U=0 \quad \frac{\partial \Theta}{\partial X}=0 \quad \frac{\partial V}{\partial X}=0 \tag{16}$$

On the opening (X=1):

$$P=P_{\infty}-U^{2} \quad \frac{\partial V}{\partial X}=0 \quad \frac{\partial U}{\partial X}=-\frac{\partial V}{\partial Y} \tag{17}$$

$$\Theta=1 \text{ if } U<0\,, \quad \frac{\partial \Theta}{\partial X}=0 \text{ if } U\geq 0$$

Emissivity value of all walls are measured by TEMP 2000A at 300K, and surface temperature of quartz lamp are unknown which obtained by the solution of Equation (12). For a thin plate with thickness of order of millimeter (t ~ 10^{-3} m) and high thermal conductivity like steel plate sheets (k ~ 10^{2} w/mK) in a natural convection regime (h~ 10 m^2K/w), the biot number is about (Bi ~ 10^{-4}) so it can be assumed that there is no temperature difference through the depth of the solid and the condition (dT/dy) = 0 is placed at the heated wall. Also as measured in experiments the maximum temperature difference between two sides of the plate is less than 5 degree of Celsius in comparison with 630 degree of Kelvin for the temperature at point (<0.01). The universality of the conclusions which presented here are not depend on the plate thickness, properties (specially thermal conductivity) and external conditions to generalize to other engineering applications which have small Biot numbers.

5.2 NUMERICAL METHOD AND BENCHMARK

In order to solve the nonlinear governing equations a computer code based on SIMPLE finite volume is generated and utilized [39]. Current code was used in [36-37] to investigate the same thermal heating problem numerically. A converged solution is obtained by iterating in time until variations in the primitive variables between subsequent iteration meet:

$$\sum\left|\phi_{i,j}^{old}-\phi_{i,j}\right|<10^{-4} \tag{18}$$

where φ stands for U, V,P, and θ. Also the under relaxation coefficient is set to 0.8, 0.8, 0.3, and 0.95 respectively. All grids are Uniform in X and Y. The grid independency is performed for grid sizes between 0.1 to 0.005 and result are presented in Table 4. A grid size of 0.01 is selected where the deviation between 0.01 and 0.005 for Nu is about 0.02 %. In order to verify the result the code is validated against the results given by de Vahl Davis [40] and Dixit and Babu [41]. Results are obtained using $\Delta X = \Delta Y = 0.02$ mesh size at $Ra = 10^4$ and $\Delta X = \Delta Y = 0.1$ at $Ra = 10^5$, 10^6. There is a maximum of 6 % deviation in Nu as shown in Table 5.

Table 4. Grid convergence study at ζ = 55.31 with N=11, A=1

ΔX	Nu	%	Ψ_{max}	%
0.1	53.12	9.5522	285.46	2.3668
0.05	57.37	2.3157	274.93	1.4093
0.01	58.72	0.0170	280.15	0.4626
0.005	58.73	0.0	278.86	0.0

Table 5. Verification study with the benchmarks

Ra	Nu		
	a	b	This study
10^3	1.116	1.120	1.13
10^4	2.242	2.286	2.25
10^5	4.531	4.563	4.54
10^6	9.035	8.800	8.9

a) de Vahl Davis [8] and b) Dixit and Babu [23].

6. NUMERICAL RESULTS

To perform less experiment a numerical code is developed. Figure 8 depicts the isotherms, streamline and vortex line of open cavity with one heat sources. In Figure 8, streamlines point up that the fluid enters the cavity from the lower part of the opening, rises along the symmetry line and following the upper horizontal boundary exits at the upper part of the opening. As expected, the flow pattern changes when the effects of thermal radiation are included the streamlines are weaker through the domain. Being more distorted by the heat sources. Analysis of the velocity field demonstrates that the derivative fields of the velocity the overall behavior of the flow structure. The comparison of numerical (continuous line) versus experimental (singular points) for maximum temperature of plate for one heat source element is shown in Figure 9. Because of assuming adiabatic boundary condition at top wall and 2-D simulations the numerical values aren't equal to experimental but they are at good agreement. By using semi-experimental general function the fitted curve of numerical results from Figure 9 is obtained as

$$T_{\max} = 113.6\left(\frac{Q}{H^2}\right)^{0.1171} \quad (19)$$

in this numerical correlation coefficients obtained with 95% root square error. Dimensionless streamline and isotherm of three lamps arrangement for case 10 of Table 5 is shown in Figure 10. Also the prediction of Equation (19) for maximum temperature of various cases is presented in Table 5.

a)

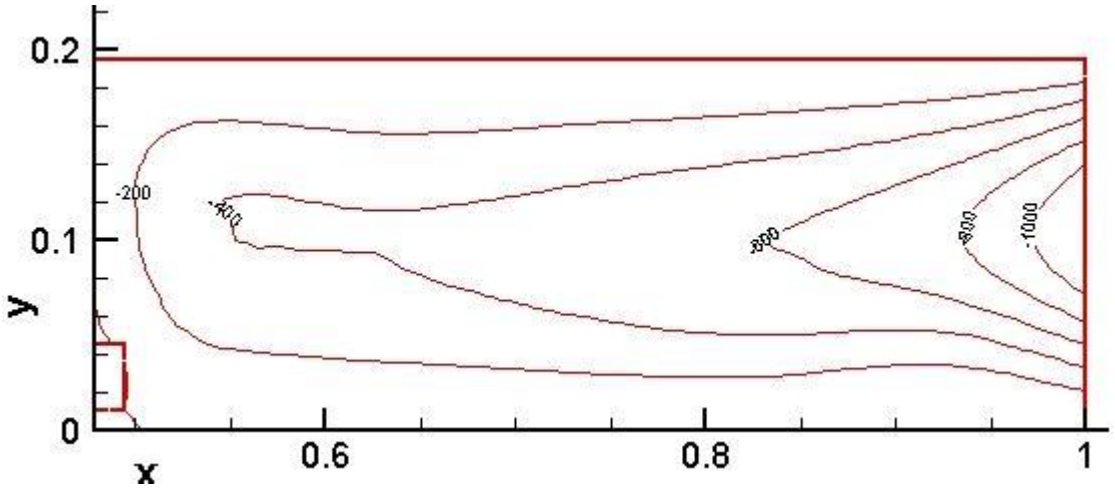

b)

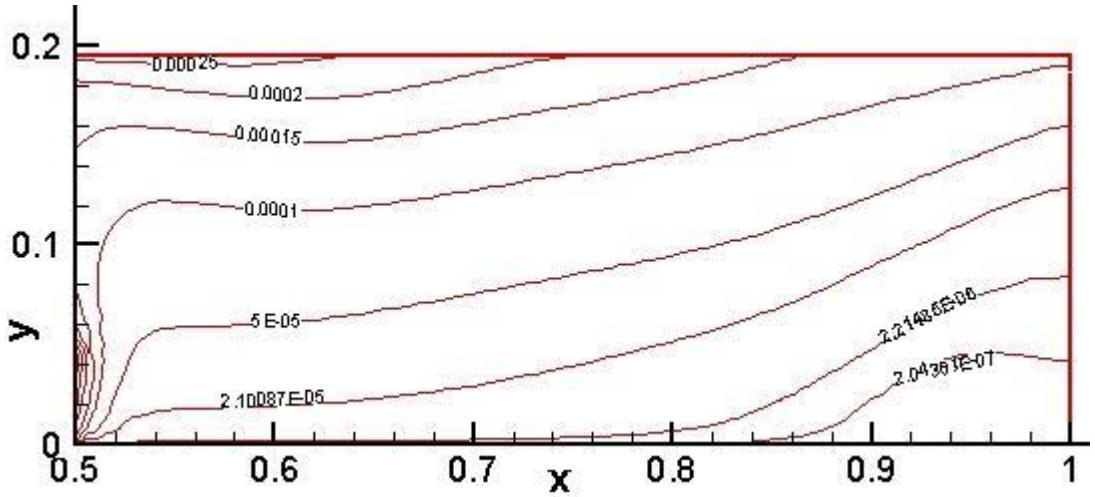

Figure 8. Dimensionless a) Streamline b) isotherm of one lamp (Q=1770 W,H= 19.5 cm)

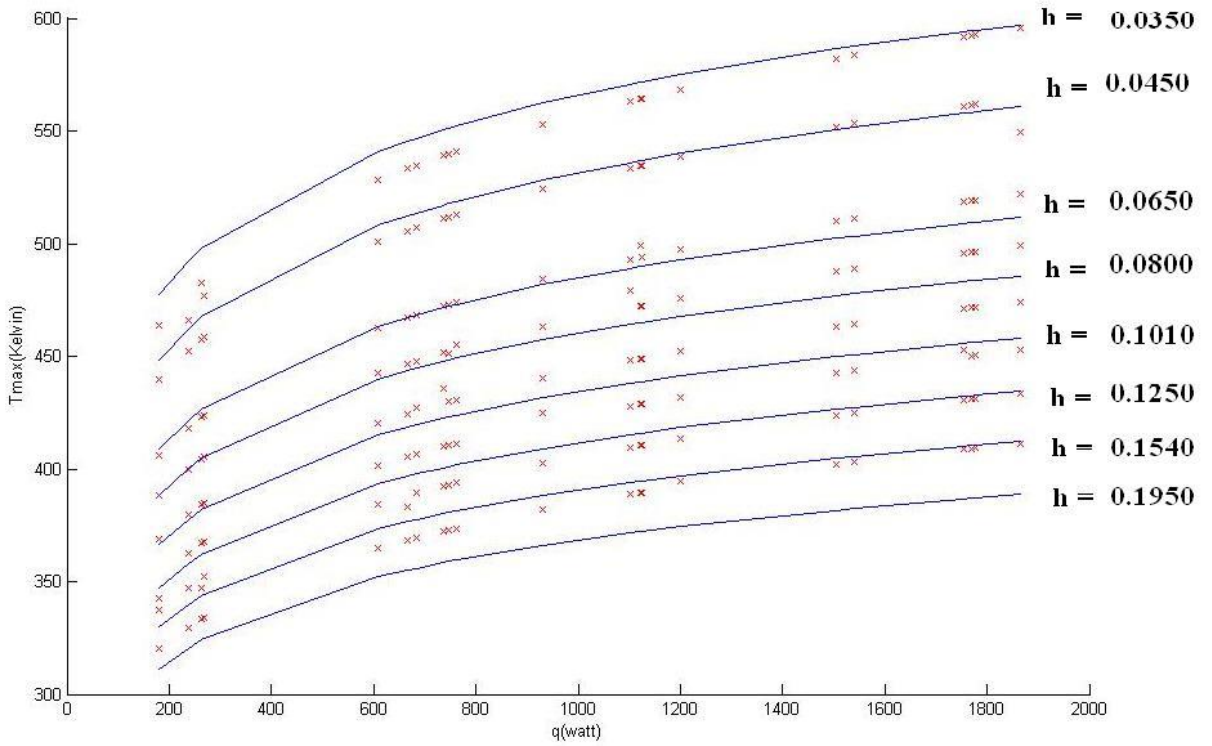

Figure 9. Numerical (Continuous line) versus experimental (singular points) comparison

a)

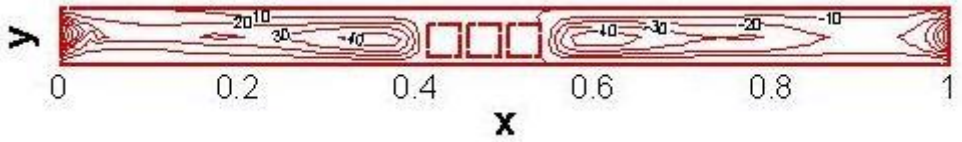

b)

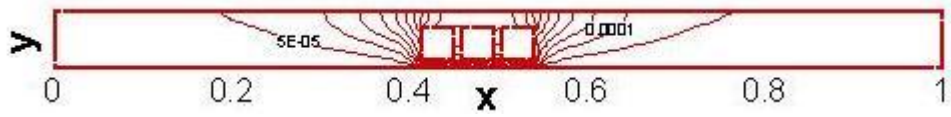

Figure 10. Dimensionless a) Streamline b) isotherm of three lamps (P1=417 W,P2=298 W,P3=366 W,H= 3.5 cm)

7. LENGTH OF UNIFORM HEAT FLUX REGION

Heat flux uniformity coefficient is defined as the ratio of minimum heat flux to maximum heat flux at uniform heat flux region. Heat flux uniformity coefficient in this study assumed between 0.5 and 0.95. Figure 11-14 depicts the length of uniform heat flux region based on the geometrical and uniformity coefficient for 50000 studied cases. The horizontal distance between lamps is ranging from 1 to 20 cm with the step of 1 cm, the vertical distance of thin plate from lamp is ranging between 1 to 20 cm with the step of 1 cm, the input power to each lamp ranging 100 W to 2000 W with the step of 100 W, and number of heat sources is ranging 1 to 20 with the step of 1 lamp. In Figure 11-14 the balance point is the horizontal distance between lamps is 10 cm, the vertical distance of thin plate from lamp is 10 cm, the power of each lamp equals to 1000 W, and number of heat sources is 10. The fitted curve with relative error of 15% is as below

$$L = 0.4 + \tag{23}$$
$$-0.614\bar{\eta} - 1.9753\bar{Q} + 0.9405\bar{d} - 0.3823\bar{N} + 2.0218\bar{H}$$
$$+1.7458\bar{Q}\bar{\eta} - 0.8668\bar{\eta}\bar{d} + 0.2228\bar{\eta}\bar{N} - 1.6479\bar{\eta}\bar{H}$$
$$-0.7762\bar{Q}\bar{d} + 0.4320\bar{Q}\bar{N} - 0.9370\bar{Q}\bar{H} + 1.7222\bar{d}\bar{N}$$
$$+0.2977\bar{d}\bar{H} - 0.4104\bar{N}\bar{H} + 0.0642\bar{\eta}^2 + 1.1919\bar{Q}^2$$
$$+0.0200\bar{d}^2 + 0.2524\bar{N}^2 - 0.0894\bar{H}^2$$

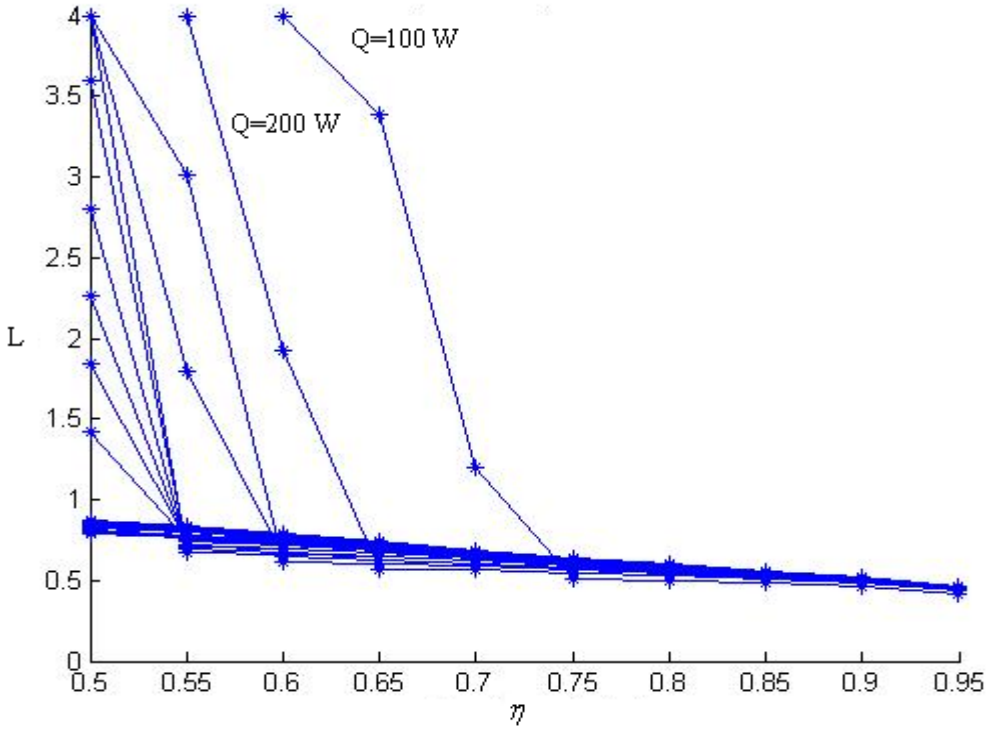

Figure 11. The length of uniform region based on power of lamps and temperature uniformity coefficient (d=10 cm,H=10 cm,N=10)

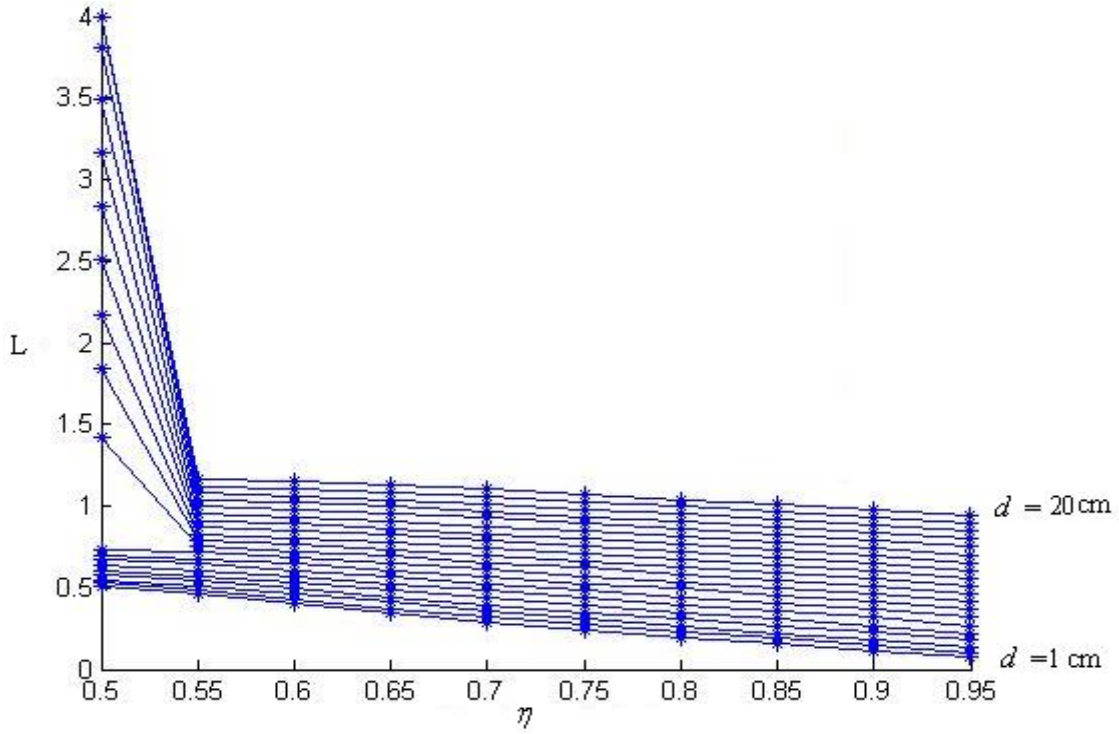

Figure 12. The length of uniform region based on distance between lamps and temperature uniformity coefficient (Q=100 W,H=10 cm,N=10)

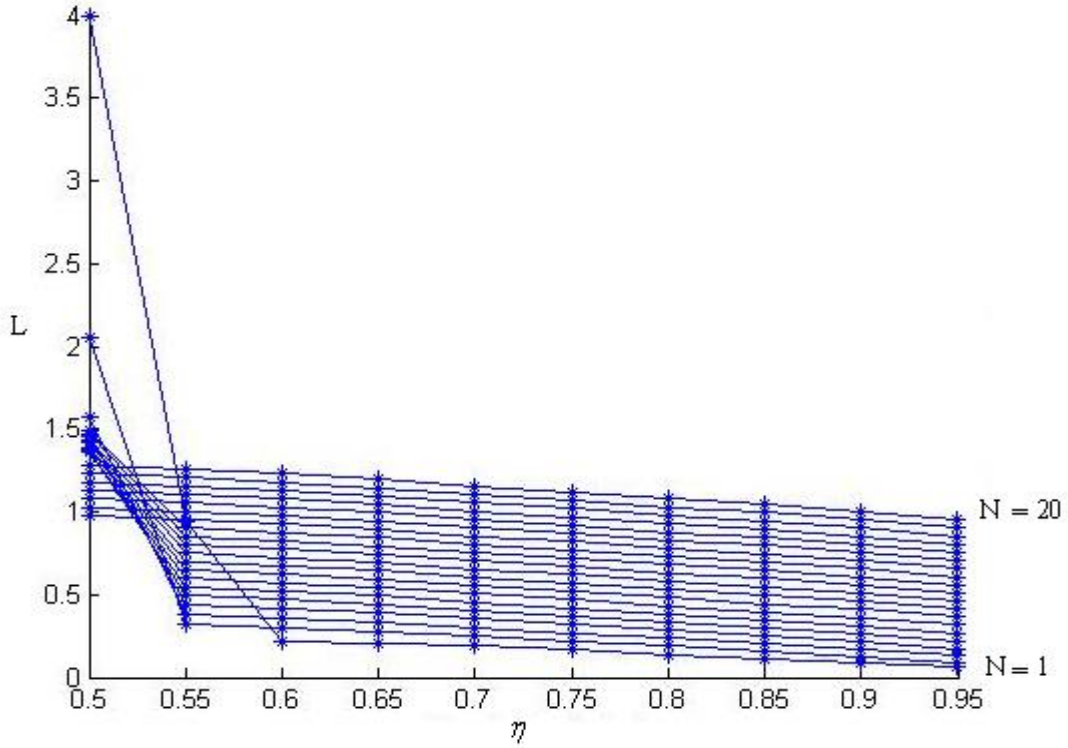

Figure 13. The length of uniform region based on number of heat sources and temperature uniformity coefficient (d=10 cm,H=10 cm,Q=1000 W)

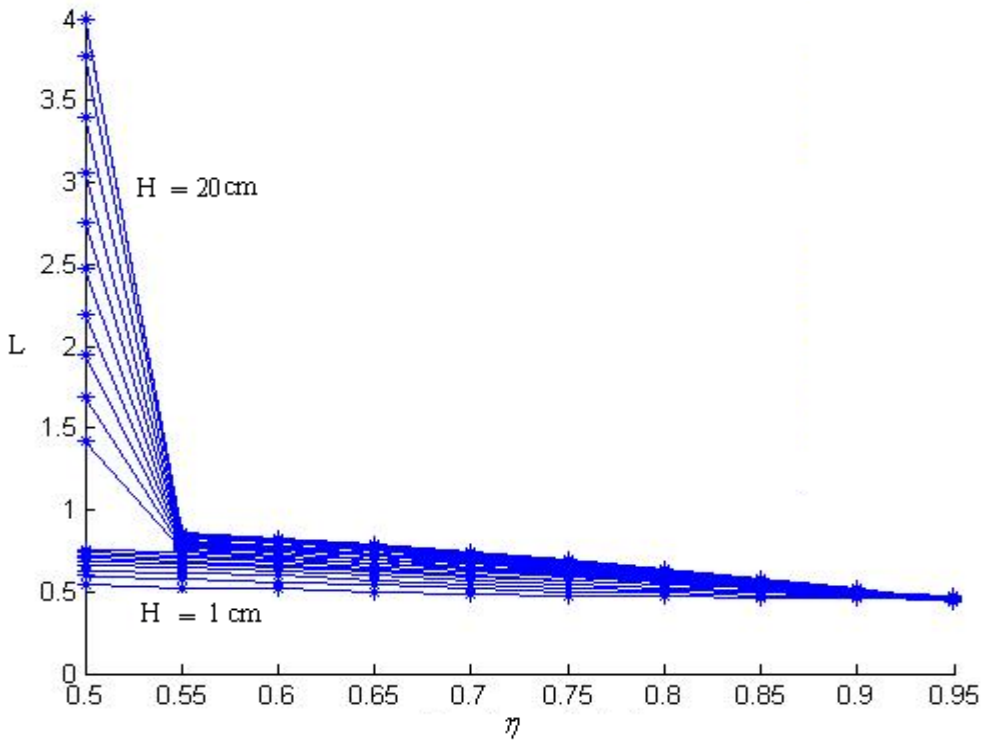

Figure 14. The length of uniform region based on Height of Plate from the Rack of Lamps and temperature uniformity coefficient (d=10 cm,N=10,Q=1000 W)

8. CONCLUSION

We investigated numerically and experimentally steady state heat transfer by natural convection and thermal radiation in an enclosure which is formed by a constant temperature wall, an adiabatic wall, two openings and discrete heat source. The most important conclusion listed as below:

- The infrared camera is a useful and precise device for the temperature measurement.
- Increasing heat source input power and decreasing aspect ratio caused the maximum temperatures increase.
- An empirical correlation developed for engineering application for the maximum temperature of heated thin plate in expose of single quartz lamp. Also by some tolerance a semi-empirical correlation and a numerical-based correlation is derived.
- Experiments have been backed up by a 2-D numerical analysis of fluid flow and heat transfer for geometry corresponds to the one used for the experiments and boundary condition based on experimental results. The good agreement between the experiments and the numerical results confirms the sufficiency of the two dimensional approximation and adiabatic wall BC (neglect the effect of conduction) at small Biot numbers for heating of a thin plate inside an open cavity using thermal radiative heat sources.
- Based on the numerical and experimental correlations, a simple method (without solving complex 3-D CFD calculations) to calculate the maximum temperature of plates for an arbitrary arrangement of heat sources is presented and verified.
- A parametric study in thermal and geometrical parameters effects on achieving a constant temperature distribution for various deviations from uniformity is illustrated.
- The effective parameter in for a uniform temperature distribution on plate are aspect ratio (the vertical distance of thin plate from lamp),input power to each lamp, the horizontal distance between lamps, uniformity coefficient, and number of heat sources respectively.
- The most effective interaction between parameters in the length of uniform temperature distribution on plate is the interaction of input power to each lamp and uniformity coefficient. Also input power to each lamp has the greatest order between quadratic terms.

9. REFERENCES

[1] E. R.,Van Driest,The Problem of Aerodynamic Heating, *Aeronautical EngineeringReview*, Oct. 1956, pp. 26–41.

[2] E. V., Zoby, Approximate Heating Analysis for theWind ward Symmetry Plane of Shuttle like Bodies at Angle of Attack, in *Thermodynamics of Atmospheric Entry*, T. E. Horton (ed.), Vol. 82, *Progress in Astronautics and Aeronautics*, American Institute of Aeronautics and Astronautics, 1982, pp. 229–247.

[3] R.M., Fand, B.Y.K., Kim, A.C.C., Lam, R.T., Phan, Resistance to the Flow of Fluids through Simple and Complex Porous Media whose Matrices are Composed of Randomly Packed Spheres, *Journal of Fluid Engineering, Transaction of ASME*, **109**, pp. 268-274 (1987).

[4] M.Y., Abdollahzadeh Jamalabadi, Effects of micro and macro scale Viscous Dissipations with Heat Generation and Local Thermal Non-Equilibrium on Thermal Developing Forced Convection in saturated porous media, Journal of Porous Media , **18**, 9, pp. 843-860 (2015) .

[5] M.Y., Abdollahzadeh Jamalabadi, Joule Heating in Low-Voltage Electroosmotic with Electrolyte containing nano-bubble mixtures through Microchannel Rectangular Orifice, *Chemical Engineering Research and Design*, **102,** 407-415 (2015).

[6] M.Y., Abdollahzadeh Jamalabadi, M.Ghasemi, M.H., Hamedi, Two-dimensional simulation of thermal loading with horizontal heat sources, *Proceedings of the Institution of Mechanical Engineers, Part C: Journal of Mechanical Engineering Science*, **226,** 1302-1308 (2012).

[7] A., Shahidian, M., Ghassemi, S., Khorasanizade, M., Abdollahzade, G., Ahmadi, Flow Analysis of Non-Newtonian Blood in a Magnetohydrodynamic Pump, *IEEE Transactions on Magnetics*, **45**, 6, 2667-2670 (2009).

[8] M.Y., Abdollahzadeh Jamalabadi, J.H., Park, M.M., Rashidi, J.M., Chen, Effects of Thermal Boundary Conditions on the Joule Heating of Electrolyte in a Microchannel, Journal of Hydrodynamics, Ser. B, accepted for publication (2015).

[9] M. S., Shadloo, R., Poultangari, M.Y., Abdollahzadeh Jamalabadi, M.M., Rashidi, A New and Efficient Mechanism for Spark Ignition Engines, *Energy Conversion and Management*, **96**, 418-429 (2015).

[10] M.Y., Abdollahzadeh Jamalabadi, J.H., Park, C.Y., Lee, Optimal Design of MHD Mixed Convection Flow in a Vertical Channel with Slip Boundary Conditions and Thermal Radiation Effects by using Entropy Generation Minimization Method, *entropy*, **17**, 2, 866-881 (2015).

[11] M.Y., Abdollahzadeh Jamalabadi, J.H., Park, Effects of Brownian motion on Freezing of PCM Containing Nanoparticles, *Thermal Science*, OnLine-First Issue 00 94-94 (2014).

[12] M.Y., Abdollahzadeh Jamalabadi, J.H., Park, C.Y., Lee, Thermal Radiation effects on the Onset of Unsteadiness of Fluid Flow in Vertical Microchannel Filled with Highly Absorbing Medium, *Thermal Science*, OnLine-First Issue 00, 124-124 (2014) .

[13] M.Y., Abdollahzadeh Jamalabadi, M., Ghasemi, M.H., Hamedi, Numerical Investigation of Thermal Radiation Effects on Open Cavity with Discrete Heat Sources, *International Journal of Numerical Methods for Heat and Fluid Flow*, **23**, 4, 649-661 (2013).

[14] M.Y., Abdollahzadeh Jamalabadi, Electrochemical and exergetic modeling of a CHP system using tubular solid oxide fuel cell and mini gas turbine , *Journal of Fuel Cell Science Technology*, **10**, 5, 051007 (2013).

[15] M.Y., Abdollahzadeh Jamalabadi, Optimal Design of Cylindrical PBX by Entransy Dissipation Extremum Principle, *International Journal of Energetic Materials and Chemical Propulsion*, accepted for publication, 15 (2016).

[16] M.Y. Abdollahzadeh Jamalabadi, Thermal Radiation Effects on Creep Behavior of the Turbine Blade, *Multidiscipline Modeling in Materials and Structures*, minor revision (2016).

[17] S., Bita, M.Y., Abdollahzadeh Jamalabadi, M., Mesbah, Toxicity study of silver nanoparticles synthesized using seaweed Sargassum angustifolium in common carp, Cyprinus carpio, *Journal of Chemical and Pharmaceutical Research*, accepted for publication (2015).

[18] M.Y. Abdollahzadeh Jamalabadi, Entropy generation in boundary layer flow of a micro polar fluid over a stretching sheet embedded in a highly absorbing medium, *Frontiers in Heat and Mass Transfer*, **6,** 1, 1-13 (2015).

[19] M.Y., Abdollahzadeh Jamalabadi, The frequency response of a cavitating hydrofoil, *Noise and Vibration Worldwide*, **45**, 8, 21-27 (2014).

[20] M.Y., Abdollahzadeh Jamalabadi, Analytical study of Magnetohydrodynamic propulsion stability, *Journal of Marine Science and Application*, **13**, 3, 281-290 (2014).

[21] M.Y., Abdollahzadeh Jamalabadi, Experimental investigation of thermal loading of a horizontal thin plate using infrared camera, *Journal of King Saud University – Engineering Sciences*, **26**, 2, 159-167 (2014).

[22] M.Y., Abdollahzadeh Jamalabadi, J.H., Park, C.Y., Lee, Economic and environmental modeling of a micro gas turbine and solid oxide fuel cell hybrid combined heat and power system, *International Journal of Applied Environmental Sciences*, **9**, 4, 1769-1781 (2014).
[23] M.Y., Abdollahzadeh Jamalabadi, Simulation of electrochemical impedance spectroscopy of a solid oxide fuel cell anodes, *World Applied Sciences Journal*, **32**, 4, 667-671 (2014).
[24] M.Y., Abdollahzadeh Jamalabadi, J.H., Park, Investigation of property variations on freezing of pcm containing nanoparticles, *World Applied Sciences Journal*, **32**, 4, 672-677 (2014).
[25] M.Y., Abdollahzadeh Jamalabadi, Economic and environmental modeling of a MGT-SOFC hybrid combined heat and power system for ship applications, *Middle-East Journal of Scientific Research*, 22, 4, 561-574 (2014).
[26] M.Y., Abdollahzadeh Jamalabadi, MD simulation of Brownian motion on trapping of Buckminsterfullerene in nano-Optical tweezers, *International Journal of Optics and Applications*, **5**, 5 161-167 (2015).
[27] M.Y., Abdollahzadeh Jamalabadi, Numerical investigation of thermal radiation effects on electrochemical impedance spectroscopy of a solid oxide fuel cell anodes, *Materials Performance and Characterization*, DOI: 10.1520/MPC20140062 (2015).
[28] M.Y., Abdollahzadeh Jamalabadi, Effect of fuel inject angle on the thermal behavior of a 2D axisymmetric non-premixed methane–air flame in vertical cylinder filled by porous media, *International Journal of Energy Engineering*, **5**,1, 1-8 (2015).
[29] M.Y., Abdollahzadeh Jamalabadi, J.H,. Park, Thermal radiation, joule heating, and viscous dissipation effects on mhd forced convection flow with uniform surface temperature, *Open Journal of Fluid Dynamics*, **4**, 2, 125-132 (2014).
[30] M.Y. Abdollahzadeh Jamalabadi, Effect of fuel inject angle on non-premixed combustion of air/methane mixtures in vertical cylinder, International Journal of Multidisciplinary Research and Development, **1**, 5, 1-4 (2014).
[31] M.Y., Abdollahzadeh Jamalabadi, J.H., Park, Electro-Magnetic Ship Propulsion Stability under Gusts, *International Journal of Sciences: Basic and Applied Research Sciences*, **1**, 421-427 (2014).
[32] M.Y., Abdollahzadeh Jamalabadi, P., Hooshmand, B., Khezri, A., Radmanesh, Investigation of using different fluids for using in gas turbine- Rankine cycle, *Indian journal of Scientific Research*, **2**, 74-81 (2014).
[33] S., Dousti, J., Cao, A., Younan, P., Allaire, T., Dimond, Temporal and Convective Inertia Effects in Plain Journal Bearings With Eccentricity, Velocity and Acceleration, *Journal of tribology*, **134**, 3, 031704,8 (2012).
[34] A., Joghataie, M. S., Dizaji, Nonlinear analysis of concrete gravity dams by neural networks, *In Proceedings of the World Congress on Engineering* (Vol. 2), (2009).
[35] F., He, P.E., Allaire, S., Dousti, A., Untaroiu, Forced response of a flexible rotor with squeeze film damper under parametric change, *ASME Turbo Expo 2013: Turbine Technical Conference and Exposition*, 1 (2013).
[36] S., Dousti, R.L., Fittro, An Extended Reynolds Equation Including the Lubricant Inertia Effects: Application to Finite Length Water Lubricated Bearings, *ASME Turbo Expo 2015: Turbine Technical Conference and Exposition* (2015).
[37] E., Sarshari, N., Vasegh, M., Khaghani, S., Dousti, Sliding Mode Control in Ziegler's Pendulum With Tracking Force: Novel Modeling Considerations, *ASME 2013 International Mechanical Engineering Congress and Exposition* (2013).
[38] S., Dousti, T.W., Dimond, P.E., Allaire, H.E., Wood, Time Transient Analysis of Horizontal Rigid Rotor Supported With O-Ring Sealed Squeeze Film Damper, *ASME 2013 International Mechanical Engineering Congress and Exposition* (2013).
[39] S., Dousti, M.A., Jalali, In-Plane and Transverse Eigenmodes of High-Speed Rotating Composite Disks, *Journal of Applied Mechanics*, **80**, 1, 011019 (2013).
[40] H., Jafarzadeh, S., Gholami, R., Bashirzadeh. A new effective algorithm for on-line robot motion planning. *Decision Science Letters*, **3**, 1, 121-130 (2014).
[41] R., Hasani, R., H., Jafarzadeh, and F., Khoshalhan, A new method for supply chain coordination with credit option contract and customers' backordered demand.Uncertain Supply Chain Management, 1(4), 207-218 (2013).
[42] A., Hassanzadeh, L., Mohseninezhad, A., Tirdad, F., Dadgostari, H., Zolfagharinia, Location-routing problem. In Facility Location, pp. 395-417. Physica-Verlag HD (2009).
[43] J. A., Kaplan, S., Dousti, P. E., Allaire, B. R., Nichols, T. W., Dimond, A. Untaroiu, Rotor Dynamic Modeling of Gears and Geared Systems. *In ASME Turbo Expo 2013: Turbine Technical Conference and Exposition* (2013).

[44] S., Dousti, J.A., Kaplan, F., He, P.E., Allaire, Elastomer O-Rings as Centering Spring in Squeeze Film Dampers: Application to Turbochargers, *ASME Turbo Expo 2013: Turbine Technical Conference and Exposition*,2 (2013).

[45] A., Joghataie, M. S., Dizaji, Designing High-Precision Fast Nonlinear Dam Neuro-Modelers and Comparison with Finite-Element Analysis, *Journal of Engineering Mechanics*, 139(10), 1311-1324, (2012).

[46] M., Hosseininia, F., Dadgostari, Connectivity. *In R. Farahani, & E. Miandoabchi (Eds.) Graph Theory for Operations Research and Management: Applications in Industrial Engineering* (pp. 37-47). Hershey, PA: Business Science Reference. doi:10.4018/978-1-4666-2661-4.ch004, (2013).

[47] M., Hosseininia, F., Dadgostari, Hamiltonian Paths and Cycles.In *Graph Theory for Operations Research and Management: Applications in Industrial Engineering: Applications in Industrial Engineering*, 96, (2012).

[48] R. Z., Farahani, F., Dadgostari, and A., Tirdad, Future Trends in SCM.*Supply Chain Sustainability and Raw Material Management: Concepts and Processes: Concepts and Processes*, 82 (2011).

[49] F., Dadgostari, M., Hosseininia, Phasing of Traffic Lights in Urban Intersections. *Graph Theory for Operations Research and Management: Applications in Industrial Engineering: Applications in Industrial Engineering*, 257 (2012).

[50] A., Joghataie, and M. S., Dizaji. Transforming results from model to prototype of concrete gravity dams using neural networks." *Journal of Engineering Mechanics* (2010).

[51] M, Farrokh, and M. S. Dizaji. Adaptive simulation of hysteresis using neuro-Madelung model, *Journal of Intelligent Material Systems and Structures*: 1045389X15604283 (2015).

[52] A., Joghataie, and M. S., Dizaji. Reducing extent of cracks and increasing time to failure of concrete gravity dams by optimization of properties of layers of concrete." *Scientia Iranica. Transaction A, Civil Engineering* 21.1 67, (2014).